ACS APPLIED MATERIALS & INTERFACES
Research Article
www.acsami.org

Electrochemical Sensing of Nitric Oxide with Functionalized Graphene Electrodes

Yifei M. Liu,[†] Christian Punckt,[†,‡] Michael A. Pope,[†,‡] Alan Gelperin,[§] and Ilhan A. Aksay*,[†]

[†]Department of Chemical and Biological Engineering and [§]Program in Neuroscience, Department of Molecular Biology, Princeton University, Princeton, New Jersey 08544, United States

[‡]Vorbeck Princeton Research Center, Vorbeck Materials Corp., 11 Deerpark Drive #203, Monmouth Junction, New Jersey 08852, United States

S *Supporting Information*

ABSTRACT: The intrinsic electrocatalytic properties of functionalized graphene sheets (FGSs) in nitric oxide (NO) sensing are determined by cyclic voltammetry with FGS monolayer electrodes. The degrees of reduction and defectiveness of the FGSs are varied by employing different heat treatments during their fabrication. FGSs with intermediate degrees of reduction and high Raman I_D to I_G peak ratios exhibit an NO oxidation peak potential of 794 mV (vs 1 M Ag/AgCl), closely matching values obtained with a platinized Pt control (791 mV) as well as recent results from the literature on porous or biofunctionalized electrodes. We show that the peak potential obtained with FGS electrodes can be further reduced to 764 mV by incorporation of electrode porosity using a drop-casting approach, indicating a stronger apparent electrocatalytic effect on porous FGS electrodes as compared to platinized Pt. Taking into consideration effects of electrode morphology, we thereby demonstrate that FGSs are intrinsically as catalytic toward NO oxidation as platinum. The lowered peak potential of porous FGS electrodes is accompanied by a significant increase in peak current, which we attribute either to pore depletion effects or an amplification effect due to subsequent electrooxidation reactions. Our results suggest that the development of sensor electrodes with higher sensitivity and lower detection limits should be feasible with FGSs.

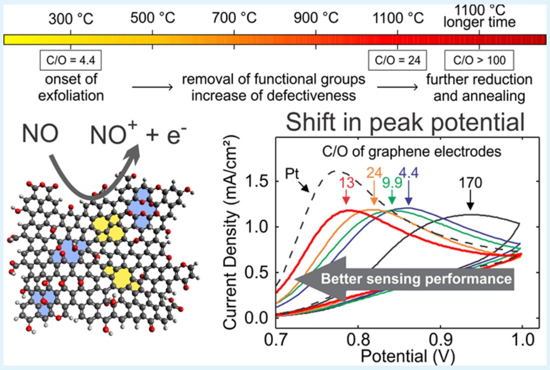

KEYWORDS: *nitric oxide, electrochemical sensing, intrinsic reactivity, functionalized graphene, porosity, electroanalysis*

■ INTRODUCTION

Nitric oxide (NO) is an intracellular messenger molecule involved in functions of the immune system, a vasodilation pathway, and communication in the nervous system.[1−3] Monitoring the evolution of NO concentration over time and with spatial resolution on the micrometer scale is crucial to elucidating the metabolic pathways and biological processes in which NO participates.[4,5] NO is a free radical and thus highly reactive toward molecular oxygen, peroxides, radicals, and metals, including metal centers such as hemoglobin.[6,7] Furthermore, NO is a small and electrically neutral molecule with a diffusion coefficient nearing 3.3×10^{-5} cm^2 s^{-1} in physiological buffer which enables NO to permeate biological membranes and diffuse quickly.[8] NO is found at low (<nM) concentrations and in conjunction with many other molecules in biological media, and its concentration changes on time scales of seconds.[5] These characteristics make NO challenging to detect with high spatial and temporal resolution.[9,10]

To date, a variety of techniques have been used to detect NO in media such as cell cultures and tissues. Broadly speaking, they are based on spectroscopic methods, such as the indirect Griess assay to measure the production of nitrite by the reaction of NO, or based on electrochemistry.[5,11] Spectroscopic approaches require large volumes of analyte and specific chemical labels, cannot detect NO production in real time, and tend to be expensive.[4] Electrochemical sensing is best suited for real-time NO detection in biological media because it requires only small volumes of analyte and is capable of providing spatially resolved NO concentration data at low analyte concentrations.[5]

Electrochemical sensing of NO is based upon the electrooxidation of NO to NO$^+$ at the sensor electrode in a one-electron process which is followed by a homogeneous reaction forming nitrite (NO$_2^-$)[5]:

$$NO \rightarrow NO^+ + e^-$$

$$NO^+ + OH^- \rightarrow HNO_2 \rightarrow H^+ + NO_2^-$$

NO_2^- is electrochemically active and may undergo subsequent electrochemical oxidation at the sensor electrode to nitrate according to $NO_2^- + H_2O \rightarrow NO_3^- + 2H^+ + e^-$, and this

Received: September 13, 2013
Accepted: November 8, 2013
Published: November 8, 2013

reaction proceeds at a similar electrochemical potential as the oxidation of NO.[12,13]

Commercial electrochemical sensor electrodes are primarily based on activated carbon fiber or noble metals (particularly platinum)[5,14,15] and require high electrochemical potentials to drive the electrooxidation reaction at a significant rate. This limits device durability and selectivity because a larger number of interfering biological species can react at high potentials, leading to increased fouling and promoting electrode deterioration.[4,5] Furthermore, high overpotentials negatively affect the signal-to-noise ratio (detection limit), and the use of noble metals such as platinum renders the sensors commercially less attractive. Research efforts to improve upon existing sensing platforms therefore seek to lower the overpotentials necessary for NO oxidation by employing electrode materials that are catalytic toward the oxidation of NO while avoiding the use of noble metals.

Recently, carbon nanotubes (CNTs) and graphene, particularly in functionalized form, have received a great deal of interest because of their electrochemical stability, high specific surface area, and demonstrated catalytic properties toward a wide variety of biomolecules and other electrochemical analytes.[16−19] Functionalized graphene sheets (FGSs) hold promise as a superior electrode material as they combine the high surface area and reactivity of nanoscale carbonaceous materials with scalability, processability, and tunability of chemical properties. FGSs can be produced by chemical[20−22] or electrochemical[23] reduction of graphene oxide or by the thermal exfoliation and reduction of graphite oxide (GO).[24,25] GO is made by chemically oxidizing graphite via routes such as the Staudenmaier method[26] or the Hummers method.[27] When GO is rapidly heated during thermal exfoliation and reduction, carbon dioxide, carbon monoxide, water, and other species evolve and exfoliate the material into mostly single sheets as the oxygen-containing functional groups are reduced.[24,25] As a result, an electrically conducting material is obtained that contains both lattice defects and the remaining oxygen groups (Figure 1a), both of which are believed to give rise to its catalytic properties in many electrochemical applications.[19,28−30] By exfoliating GO at different temperatures in the range from 300 to 1100 °C, the concentration and the type of oxygen-based functional groups and lattice defects in the resulting FGSs can be modified, i.e., the degree and the type of functionalization and defectiveness can be tuned.[31] Prolonged treatment at temperatures in excess of 1500 °C causes the lattice defects to heal, eventually leading to the re-establishment of the sp^2-hybridized hexagonal pristine graphene structure.[32] The elemental composition of FGSs can be described by the carbon-to-oxygen ratio (C/O), with $C/O \approx 2$ for graphene oxide and $C/O \rightarrow \infty$ for pristine graphene. We denote FGSs with $C/O = x$ as FGS_x to indicate their degree of reduction.

For use in electrochemical NO sensing, FGSs have previously been fabricated into electrodes through a variety of different approaches: graphene oxide has been drop-cast onto substrates and subsequently electrochemically reduced;[33] composite paste electrodes of mildly thermally reduced FGSs and ionic liquids (ILs) have been prepared;[34] and chemically or thermally reduced FGS-based electrodes have been modified with catalytic entities such as cytochrome c[35] and hemoglobin.[36] Such approaches lead to high-surface-area, porous electrodes. The lowest NO oxidation potentials of ~800 mV (as measured by cyclic voltammetry vs Ag/AgCl) have been achieved in the studies with thermally reduced[34] or catalyst-modified materials.[35] However, while useful electrode performances could be demonstrated, only little is understood regarding the intrinsic electrocatalytic properties of these materials since their performance is typically strongly affected by morphological factors, i.e., electrode roughness and porosity[37] which have not been accounted for in previous studies. Contributions of morphological effects were pointed out in earlier studies of the general redox activity of carbonaceous nanomaterials[38] and discussed in theoretical and experimental work by Compton and co-workers.[39−41] Nonetheless, in experimental studies, in most cases, it is overlooked that the large electrolyte-accessible specific surface area of rough or porous electrodes can result in a higher apparent rate of reaction and thus more sensitive detection. Electrode morphology is not well-defined, and apparent "catalytic" effects are erroneously attributed solely to high intrinsic catalytic activity of the electrode material.

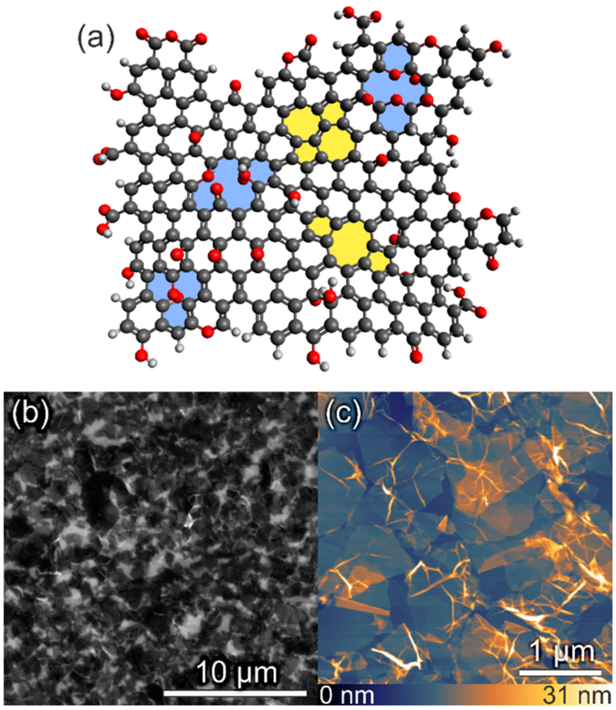

Figure 1. (a) FGS schematic, showing examples for lattice defects (yellow, topological defects; blue, oxygen-decorated vacancy defects) and oxygen-containing functional groups (O atoms shown in red). (b) SEM image of a monolayer of FGS_{24} on a gold substrate. (c) Contact mode AFM image of a monolayer of $FGS_{4.4}$ on mica.

To study the reactivity of the FGSs independently of extrinsic effects such as roughness and porosity, we recently developed an approach to test the electrochemical properties of FGS monolayer (ML) electrodes.[42] Since the morphology of these ML electrodes is well-defined and to a first approximation resembles that of a flat electrode,[42] the electrode performance can be attributed to the intrinsic reactivity of the FGSs.[37] In the following, we measure the intrinsic electrocatalytic properties of FGS ML electrodes fabricated with different degrees of thermal reduction toward the oxidation of NO by cyclic voltammetry. We compare the results with the performance of platinized Pt electrodes. By electrochemically analyzing the roughness and porosity of the platinum electrode and by comparison with drop-cast, highly porous FGS electrodes, we demonstrate that FGSs show catalytic properties equal to those of platinum, and that by further optimization of the electrode morphology the development of sensor electrodes with higher sensitivity and lower detection limits should be feasible.

MATERIALS AND METHODS

FGS Preparation. GO was produced by oxidizing flake graphite powder either according to the Staudenmaier method[26] or by an improved Hummers process.[43] FGSs were prepared by simultaneous exfoliation and reduction of GO inside a tube furnace (Lindberg Blue M) for 60 s at various temperatures between 300 and 1100 °C under vacuum. Staudenmaier GO was exfoliated at 300, 900, and 1100 °C and used as produced. FGSs exfoliated at 1100 °C were also reduced further for 60 min at 1100 °C under argon in a resistively heated graphite furnace (Astro-1000, Thermal Technologies). Hummers GO was exfoliated for 60 s at 1100 °C.

FGS Characterization. The C/O was estimated by energy-dispersive X-ray spectroscopy (EDS, INCA x-act, Oxford Instruments, UK) using a VEGA1 scanning electron microscope (SEM, Tescan USA). For EDS, dense pellets of FGSs were prepared by compression of ~10 mg of material in a 5 mm diameter pellet pressing die.

Raman spectroscopy (Kaiser Optics, λ = 532 nm) was carried out on samples prepared in the same way as for EDS analysis. The D and G peaks were fit to a Lorentzian and Breit-Wigner-Fano line shape, respectively.[44] The fitted peaks were integrated to determine the I_D to I_G peak ratio (I_D/I_G) of the materials.

Electrode Fabrication. FGS ML electrodes were prepared on gold and highly oriented pyrolytic graphite (HOPG) substrates as described previously.[42] The gold substrates were 10 mm × 10 mm pieces of silicon wafer coated with a 10 nm Ti adhesion film, a 100 nm Pt diffusion barrier and a final 300 nm Au layer using an ebeam evaporator (Angstrom Engineering). Prior to coating with FGSs, gold films were annealed in a hydrogen flame for 2 s and immediately stored in deionized (DI) water. FGSs were suspended in 1,2-dichloroethane (DCE, Acros Organics) at a concentration of 0.1 g/L by tip-sonication (Vibra-cell, Sonics & Materials Inc., CT) for 30 min, followed by centrifugation at 3000 rpm for 1 h (IEC Centra GP8R centrifuge with 218A rotor). A monolayer of FGSs was deposited onto the gold and HOPG pieces using a Langmuir−Blodgett (LB) trough.[42] Samples were dried overnight under argon and used the next day. FGS-coated gold substrates were immersed in a 1 mM solution of hexadecanethiol in ethanol for 4−10 h to passivate the gold before electrochemical experiments. Copper tape was used to improve the electrical contact between the gold film and the metal sample holder for use in electrochemical experiments.

Drop-cast electrodes of up to 20 μg/cm^2 FGS loading were prepared by depositing FGS suspensions in DCE on a polished glassy carbon substrate and drying them on a hot plate at 80 °C for 30 min. The electrodes were then used for experiments without further processing. For the platinized Pt electrodes, 10 μL of 4.8 mM hexachloroplatinic acid in ethanol per cm^2 of substrate was deposited onto a fluorine-doped tin oxide (FTO) film on glass. The samples were heated in a furnace to 400 °C for 30 min. Before use, the samples were heated again to 300 °C for 30 min to remove adsorbed contaminants. Copper tape was used to electrically connect the FTO film to the metal sample holder.

Electrode Characterization. Electrodes were imaged using the SEM as well as contact-mode atomic force microscopy (AFM, Veeco Multimode with Nanoscope III controller). For AFM, monolayers of FGS were deposited on a mica substrate, which exhibits a greater degree of flatness than does HOPG or a Au substrate. Platinized Pt electrodes were further characterized using EDS.

NO Solution Preparation. Saturated NO solutions were produced by bubbling NO gas (CP grade 99%, Matheson Tri-Gas) through deoxygenated phosphate buffered saline (PBS) solution for 30 min. The solubility of NO in PBS solution has been reported to be 1.8 mM at room temperature.[33,45] Aliquots of these saturated solutions were then used to prepare 20 mM NO solution for electrochemical experiments. NO bubbling and electrochemical measurements using NO gas were carried out inside a nitrogen-filled glovebag that was located inside a fume hood. Fresh saturated solutions of NO gas were prepared for each set of experiments.

Electrochemical Measurements. Electrochemical experiments were carried out using a custom-made polytetrafluoroethylene (PTFE, Teflon) three-electrode electrochemical cell[42] using a Pt mesh counter electrode and a Ag/AgCl reference electrode (1 M KCl, 0.235 V vs the standard hydrogen electrode). All potentials in this work are reported vs a Ag/AgCl reference. To characterize the performance of the electrodes to NO oxidation, 20 mM NO gas was dissolved in deoxygenated PBS. The potential was scanned from 0 to 1.0 V at 100 mV/s. All cyclic voltammetry measurements were conducted at room temperature using a computer-controlled digital potentiostat (Model VSP, Bio-Logic USA).

For electrochemical porosity measurements, the ferro/ferricyanide redox couple was used to carry out cyclic voltammetry experiments in the quasi-reversible regime. 2.5 mM potassium ferrocyanate was dissolved in 0.1 M PBS at pH 7.4, and KCl was added to obtain a final KCl concentration of 1 M. PBS background electrolyte with 1 M KCl and without ferrocyanide was prepared to conduct background measurements. Cyclic voltammograms (CVs) of both the ferrocyanide redox couple and the background electrolyte were performed and porosity was quantified as described previously.[37] In short, the pore volume was determined by subtracting simulated CVs for a flat electrode from experimentally determined CVs of the porous electrodes. The difference in the ferrocyanide oxidation currents was used to calculate the pore volume of the electrode assuming that the current of the porous electrodes is increased because of a pore depletion effect, such that the extra charge flowing is due to only the electrolyte present within the accessible pore space of the electrode at the beginning of the cyclic voltammetry experiment.[37] Indirect indications for electrode porosity were obtained from measurements of the accessible electrode surface area based on capacitive charging during cyclic voltammetry as well as from determining the peak-to-peak separation of the ferro/ferricyanide couple that decreases with increasing electrode porosity (and roughness).[30,37,39]

RESULTS AND DISCUSSION

Intrinsic Reactivity of Monolayer Electrodes. Table 1 shows the list of materials produced with corresponding C/O and I_D/I_G. C/O ranged from 4.4 (300 °C exfoliation) to 170 (annealed material). Hummers GO exfoliated at 1100 °C had a C/O of 13, intermediate between the 900 and 1100 °C treatments of Staudenmaier GO. For the Staudenmaier material, the I_D/I_G increased with increasing exfoliation temperature up to a value of 1.78. The annealed material, on the other hand, exhibited a significantly reduced I_D/I_G of 1.32, and the FGSs produced from Hummers GO showed the largest I_D/I_G of all the FGSs tested, reaching a value of 2.01. The SEM and the AFM images of typical monolayer coatings of FGSs produced with two of these materials (FGS$_{24}$ and FGS$_{4.4}$) are shown in panels b and c in Figure 1. The FGS monolayers have the appearance of wrinkled sheets on the thiolated gold substrate and have been shown to closely approximate the

Table 1. C/O and Raman I_D/I_G for FGSs and starting materials

carbonaceous material	C/O	Raman I_D/I_G
Staudenmaier GO	2.0	
300 °C exfoliated	4.4	1.55
900 °C exfoliated	9.9	1.61
1100 °C exfoliated	24	1.78
1100 °C exfoliated and annealed	170	1.32
modified Hummers GO	1.6	
1100 °C exfoliated	13	2.01

behavior of flat electrodes, i.e., electrodes with negligible roughness and porosity.[37,42] Therefore, such ML electrodes can be used to determine the intrinsic electrocatalytic properties of FGSs.[37]

CVs of NO oxidation for the different FGS ML electrodes are shown in Figure 2a. As the C/O of the exfoliated Staudenmaier-based FGSs increased from 4.4 to 24, the oxidative peak potential decreased from 863 to 822 mV. The exfoliated and annealed FGS_{170}, on the other hand, exhibited a high peak potential of 936 mV. The modified Hummers GO-based FGS_{13} showed the lowest peak potential of 794 mV which, within measurement error, was equal to the peak potential measured with the platinized Pt control (791 mV). Although there was no clear trend of peak potential with C/O, we observed that I_D/I_G and peak potential were inversely correlated (Figure 2b): The highest peak potential was observed for the lowest I_D/I_G measured with the annealed FGS_{170}, whereas the lowest peak potential was associated with the highest measured value of I_D/I_G in the case of FGS_{13}. FGSs with intermediate I_D/I_G correspondingly showed intermediate oxidation peak potentials. To better understand the electrochemical behavior of the different types of FGSs, in the following, we discuss the structural properties of the materials and relate them to electrochemical performance.

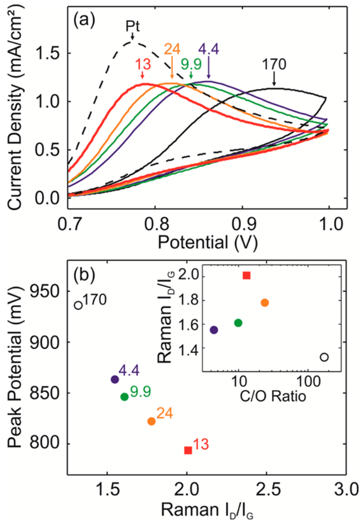

Figure 2. (a) CVs of various FGS ML electrodes in deoxygenated PBS solution with dissolved NO gas and (b) plot of NO peak potential vs I_D/I_G, with each data point labeled with the C/O of the material. Numbers next to data points in (a) and (b) indicate the C/O of the FGSs used for measurement. Peak potential appears to be inversely correlated with I_D/I_G. The inset shows I_D/I_G as a function of corresponding C/O for purpose of comparison.

The I_D/I_G gives information about the structure of the sp^2-hybridized phase within the FGSs:[44] The G-peak corresponds to stretching vibrations of individual sp^2 pairs within the graphene lattice, whereas the D-peak corresponds to the breathing mode of six-membered, sp^2-hybridized rings, a mode that is only active near defect sites (e.g., lattice defects, edges, functional groups) where the lattice symmetry is broken. Since not only individual sp^2 bonds and aromatic rings form during reduction but also defects are created as oxygen-containing functional groups are removed from the FGSs, the relation between I_D/I_G and the degree of reduction is rather complicated. It has been shown for many carbonaceous materials, including graphene, that the I_D/I_G is a nonmonotonic function of the average distance between defects (L_a) in the graphene lattice (either functional groups or lattice defects).[44] When L_a is small (<2 nm), an increase in I_D/I_G indicates the growth of pristine graphene domains. Conversely, when L_a is larger, an increase in I_D/I_G is inversely correlated with L_a. To deduce structural changes from changes in I_D/I_G, it is therefore necessary to know L_a.[44]

For FGSs with C/O < 25 (density of functional groups >1.5 O/nm^2), L_a < 0.67 nm, assuming a random distribution of functional groups. This suggests that an increase in the I_D/I_G corresponds to an increase in the number of 6-membered, sp^2-hybridized rings. However, it is not accurate to assume a random distribution of oxygen groups in FGSs as indicated by high resolution transmission electron microscopy images of clustering of sp^2 regions in reduced graphene oxide.[46,47] Therefore, our FGSs likely exhibit a lattice structure where L_a > 2 nm so that an increase in I_D/I_G would indicate an increase in material defectiveness. We therefore suggest that the significantly larger value of I_D/I_G for the FGSs produced from Hummers GO is due to an increased number of lattice defects compared to the other FGSs used in this study. This view is supported by the observation that the Hummers GO used in this study has a significantly lower C/O (∼1.6) than the Staudenmaier GO (C/O ≈ 2.0), which can be expected to lead to a larger "disruption" of the carbon lattice upon its reduction. Lastly, the low I_D/I_G of FGS_{170} can be explained by an increased L_a compared to the nonannealed materials. The increase in L_a can be the result of either (i) the removal of the majority of functional groups on the FGSs during annealing via a mechanism that does not create more lattice defects, or (ii) an alteration of the number density, type, or distribution of lattice defects.

We thus offer the following interpretation of our electrochemical data: For the Staudenmaier-based FGSs with C/O of 4.4−24, the removal of oxygen-containing functional groups with increasing exfoliation temperature increases the number density of lattice defects. Concurrently, the removal of functional groups increases the electrical conductivity of the FGSs.[42,48] Both the increase in defect density and electrical conductivity can in principle lead to improved electrochemical performance: At low C/O, the high electrical resistance of FGSs (>100 kΩ/sq in plane at C/O = 7.3)[48] can give rise to significant electron transfer resistance to the extent that the electrode becomes completely blocking (which is the case for unreduced material with C/O ≈ 2).[42] With increasing C/O, the effect of electrical resistance becomes insignificant and thus no longer impedes electron transfer. The increase in the number density of lattice defects is expected to either lead to the presence of reactive "dangling bonds" or the formation of particular functional groups decorating the edges of defect sites.[49] Lattice defect sites in CNTs have also been shown to enhance the electrochemical response arising from oxidation of NO, as well as insulin and cysteine derivatives.[50] Thus, the functional groups or dangling bonds arising from defects may help catalyze NO oxidation. This observation supports previous studies where it has been shown that different degrees of functionalization can have a pronounced effect on the electroactivity of graphene with respect to standard redox probes such as ferrocyanide.[51] However, FGS_{13} and FGS_{24} contain a smaller number density of functional groups than $FGS_{9.9}$ but at the same time exhibit a higher I_D/I_G suggesting a higher number density of lattice defects. The fact that they also exhibit an increased electrocatalytic activity toward NO oxidation suggests that lattice defects may play a more important role in catalyzing NO oxidation than functional groups.

The weaker electrochemical response observed with FGS_{170} suggests that mostly oxygen-decorated defects play an active role in NO oxidation because the processing temperature of 1100 °C is too low to cause significant lattice annealing[32] and the reduced electrochemical activity must likely be attributed to the loss of oxygen compared to nonannealed FGSs. Nonetheless, the possibility of a partial mobilization of lattice defects beginning at temperatures of 1100 °C cannot be fully excluded, and therefore a fraction of the loss of electroactivity in FGS_{170} might be attributable to a decrease in defect density as well. In summary, our results show that highly defective FGSs with intermediate C/O are effective as catalysts for NO oxidation and achieve a performance that is equal to that of our platinized Pt control and to published results obtained with catalyst-modified graphene[35,36] and IL/FGS composites.[34]

As we show in the following, the comparison between FGS MLs and platinized Pt is not a fair one: While we were probing the intrinsic electrochemical properties of the ML electrodes, the response obtained with the Pt electrode was affected by electrode roughness and porosity. To take such morphological effects into account, we performed a more detailed electrochemical characterization of our Pt electrodes and fabricated porous FGS electrodes for comparison.

Porosity Effects. A closer inspection of the CVs obtained with platinized Pt (Figure 2a) reveals that, compared to the ML electrodes, there is an increased capacitive background current as well as a significantly higher NO oxidation peak current. Significant capacitive background currents are typically observed in the literature as well.[33−36] In our case, they may partly be attributed to a higher intrinsic double layer capacitance of Pt as compared to FGSs; the accompanying increase in peak current, however, is a clear indication of electrode porosity.[37] Porosity and, to a lesser degree, roughness of an electrode effectively increase its reactive surface area and thus increase the number of reactive sites per projected electrode surface area. Because our ML electrodes exhibit practically no porosity or roughness, we conducted tests with drop-cast porous FGS electrodes to obtain a fair comparison with the intrinsically porous platinized Pt electrode as well as with literature results.

To relate electrode morphology to NO sensing characteristics, we first needed to quantify the porosity of our electrodes. To this end, we recently developed an electrochemical methodology that allows for measurement of electrode porosity in situ, using the standard redox couple ferrocyanide as outlined in more detail in the Methods section.[37] In Table 2, we show the characterization results for an FGS_{13} ML electrode and two drop-cast FGS_{13} electrodes as well as platinized Pt. All electrodes exhibited the same geometrical surface area of approximately 0.23 cm^2. According to our analysis, the drop-cast electrodes had pore volumes of 53 and 67 nL, accessible surface areas significantly larger than the electrode geometric surface area, and peak-to-peak separations lower than the theoretical limit for a reversible redox reaction on a flat electrode (∼57 mV), all of which clearly indicate the presence of significant electrode porosity.[30,37,39] For the platinized Pt electrode, we obtain a lesser but still significant degree of porosity with a cumulative pore volume of about 10 nL.

Table 2. Measured Porosities and Associated Morphological Properties for Various Electrodes, Determined Using 2.5 mM Ferrocyanide in 1 M KCl Aqueous Solution

electrode material	pore volume (nL)	E_{pp} (mV)	surface area (cm^2)
FGS ML	0	60.4	0.26
5 μg FGSs	19	65.9	1.18
10 μg FGSs	53	55.2	3.43
20 μg FGSs	67	54.3	5.40
Platinized Pt	10	56.8	1.26

The effect of pore volume on the NO oxidation response is shown in Figure 3a. The porous FGS electrodes showed peak potentials of 764 and 766 mV, i.e., significantly lower than the peak potential measured with platinized Pt. Two factors may have contributed to the lower peak potential: (i) increased accessible surface area of the electrode and (ii) electrode pore depletion. The increased surface area of the porous electrodes may have resulted in a larger number density of active sites for NO oxidation, thus resulting in an increase in the effective oxidation rate and improved sensing performance. Pore depletion, on the other hand, can occur when the pore volume and pore size limit the diffusion of the analyte into the pore network. Within the pore space, the analyte reacts away faster than it can be replenished through diffusive transport, causing an early maximum in the oxidation current.[37] Pore depletion is also expected to result in an increased peak current,[39] which was indeed observed in the CVs of the porous electrodes.[37] For the electrode with a calculated pore volume of 53 nL (based on measurement with ferrocyanide), integrating the NO oxidation current from the CV and subtracting the result from the integral of the ML, we find that a volume of 50 nL of 20 mM NO solution accounts for the extra faradaic charge transfer. This suggests that the NO contained within the electrode pores is sufficient to give rise to the observed increase in current.

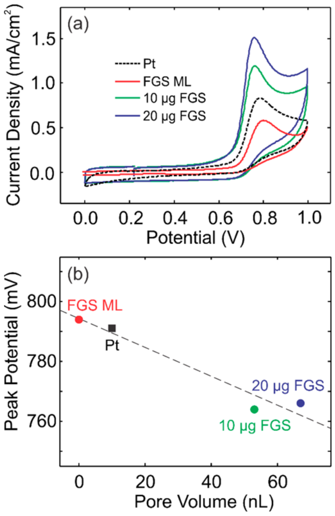

Figure 3. NO oxidation on porous FGS electrodes, with FGS ML and platinized Pt electrodes for comparison. (a) CVs of 20 mM NO gas in deoxygenated PBS. (b) NO oxidation peak potential as a function of cumulative electrode pore volume. The dashed line represents a linear fit of all data points.

This latter observation, however, may be a coincidence as another effect might also contribute to increased oxidation currents: Within the porous electrodes, the nitrite generated as a result of NO oxidation cannot diffuse away from the electrode surface as readily as it can in the case of a flat electrode, and thus the probability increases that nitrite is further electrochemically oxidized giving rise to additional faradaic currents. With NO as the analyte, this effect may be particularly relevant due to the fact that the charged nitrite ($D = 1.8 \times 10^{-5}$ cm^2 s^{-1} in water)[52] diffuses more slowly than NO. For highly porous electrodes, the nitrite oxidation current may have the same magnitude as the NO oxidation current, assuming that NO diffuses deep into the electrode such that no significant fraction of the generated nitrite can diffuse into the bulk electrolyte.

The observation that the drop-cast FGS electrodes achieved a lower peak potential than the platinized Pt baseline demonstrates that it is possible to shift peak potentials significantly by tuning the morphology of the electrode surface. When peak potential is plotted against pore volume for the platinum and FGS electrodes, the data point for platinum lies close to the curve connecting the FGS ML electrode with the porous FGS electrodes (Figure 3b). This suggests that the intrinsic reactivities of the FGSs and the platinized Pt may be similar since an FGS electrode with a pore volume equal to that of the Pt electrode can be expected to give equal performance in terms of oxidation potential. In the Supporting Information, we show additional results obtained with Pt rod electrodes using diethylamine NONOate as a source of NO in aerated electrolyte, which suggest that polished Pt exhibits less electrocatalytic activity toward NO oxidation than an FGS$_{13}$ ML electrode and thus support our above conjecture regarding the comparison of porous FGS and platinized Pt.

■ CONCLUSIONS

We investigated the intrinsic reactivity of FGS materials for NO sensing by varying the structure of the FGSs through thermal processing. FGS ML electrodes were used to eliminate the influence of morphological effects in cyclic voltammetry experiments. C/O and Raman I_D/I_G were used to infer the lattice defect and functional group density of each FGS material. More lattice defects in the FGSs resulted in greater reactivity toward NO oxidation, as indicated by lower peak potentials in the CVs. A catalytic activity of functional groups, in particular of those decorating lattice defects, is likely.

We carried out preliminary studies of the role of morphological effects in NO oxidation by fabricating porous FGS electrodes and characterizing their cyclic voltammetry response. By incorporating a small amount of porosity in FGS electrodes, it was possible to drastically improve the results obtained with ML electrodes. These improvements could be attributed either to pore depletion or the occurrence of subsequent electrochemical oxidation of nitrite. Considering these porosity effects, we concluded that FGS electrodes with intermediate C/O and high defectiveness show intrinsic electrocatalytic activity equal to that of platinized Pt. We have thereby shown that the electrocatalytic properties of FGSs toward NO oxidation rival those of more complex electrode systems involving the use of ionic liquids or heme proteins.

■ ASSOCIATED CONTENT

Ⓢ Supporting Information

Additional figure. This material is available free of charge via the Internet at http://pubs.acs.org.

■ AUTHOR INFORMATION

Corresponding Author

*E-mail: iaksay@princeton.edu.

Author Contributions

The manuscript was written through contributions of all authors. All authors have given approval to the final version of the manuscript.

Notes

The authors declare no competing financial interest.

■ ACKNOWLEDGMENTS

Funding for this work was in parts provided by the Lidow Senior Thesis Fund of the School of Engineering and Applied Science of Princeton University (Y. M. Liu).

■ REFERENCES

(1) Bredt, D. S.; Snyder, S. H. *Neuron* **1992**, *8*, 3.

(2) Wink, D. A.; Mitchell, J. B. *Free Radical Biol. Med.* **1998**, *25*, 434.

(3) Ricciardolo, F. L.; Sterk, P. J.; Gaston, B.; Folkerts, G. *Physiol. Rev.* **2004**, *84*, 731.

(4) Trouillon, R. *Biol. Chem.* **2013**, *394*, 17.

(5) Bedioui, F.; Quinton, D.; Griveau, S.; Nyokong, T. *Phys. Chem. Chem. Phys.* **2010**, *12*, 9976.

(6) Beckman, J. S.; Chen, J.; Ischiropoulos, H.; Crow, J. P. *Method. Enzymol.* **1994**, *233*, 229.

(7) Ford, P. C. *Pure Appl. Chem.* **2004**, *76*, 335.

(8) Denicola, A.; Souza, J. M.; Radi, R.; Lissi, E. *Arch. Biochem. Biophys.* **1996**, *328*, 208.

(9) Lowe, G.; Buerk, D. G.; Ma, J.; Gelperin, A. *Neuroscience* **2008**, *153*, 842.

(10) McQuade, L. E.; Ma, J.; Lowe, G.; Ghatpande, A.; Gelperin, A.; Lippard, S. J. *Proc. Natl. Acad. Sci.* **2010**, *107*, 8525.

(11) Hetrick, E. M.; Schoenfisch, M. H. *Annu. Rev. Anal. Chem.* **2009**, *2*, 409.

(12) Crespi, F.; Campagnola, M.; Neudeck, A.; McMillan, K.; Rossetti, Z.; Pastorino, A.; Garbin, U.; Fratta-Pasini, A.; Reggiani, A.; Gaviraghi, G. *J. Neurosci. Methods* **2001**, *109*, 59.

(13) Mesároš, Š. *Method. Enzymol.* **1999**, *301*, 160.

(14) Allen, B. W.; Piantadosi, C. A.; Coury, L. A., Jr. *Nitric Oxide* **2000**, *4*, 75.

(15) Lee, Y.; Oh, B. K.; Meyerhoff, M. E. *Anal. Chem.* **2004**, *76*, 536.

(16) McCreery, R. L. *Chem. Rev.* **2008**, *108*, 2646.

(17) Zhou, M.; Zhai, Y.; Dong, S. *Anal. Chem.* **2009**, *81*, 5603.

(18) Alwarappan, S.; Erdem, A.; Liu, C.; Li, C.-Z. *J. Phys. Chem. C* **2009**, *113*, 8853.

(19) Shao, Y.; Wang, J.; Wu, H.; Liu, J.; Aksay, I. A.; Lin, Y. *Electroanalysis* **2010**, *22*, 1027.

(20) Stankovich, S.; Dikin, D. A.; Piner, R. D.; Kohlhaas, K. A.; Kleinhammes, A.; Jia, Y.; Wu, Y.; Nguyen, S. T.; Ruoff, R. S. *Carbon* **2007**, *45*, 1558.

(21) Park, S.; Ruoff, R. S. *Nat. Nanotechnol.* **2009**, *4*, 217.

(22) Shin, H. J.; Kim, K. K.; Benayad, A.; Yoon, S. M.; Park, H. K.; Jung, I. S.; Jin, M. H.; Jeong, H. K.; Kim, J. M.; Choi, J. Y.; Lee, Y. H. *Adv. Funct. Mater.* **2009**, *19*, 1987.

(23) Guo, H. L.; Wang, X. F.; Qian, Q. Y.; Wang, F. B.; Xia, X. H. *ACS Nano* **2009**, *3*, 2653.

(24) Schniepp, H. C.; Li, J. L.; McAllister, M. J.; Sai, H.; Herrera-Alonso, M.; Adamson, D. H.; Prud'homme, R. K.; Car, R.; Saville, D. A.; Aksay, I. A. *J. Phys. Chem. B* **2006**, *110*, 8535.

(25) McAllister, M. J.; Li, J.-L.; Adamson, D. H.; Schniepp, H. C.; Abdala, A. A.; Liu, J.; Herrera-Alonso, M.; Milius, D. L.; Car, R.; Prud'homme, R. K. *Chem. Mater.* **2007**, *19*, 4396.

(26) Staudenmaier, L. *Ber. Dtsch. Chem. Ges.* **1898**, *31*, 1481.

(27) Hummers, W. S.; Offeman, R. E. *J. Am. Chem. Soc.* **1958**, *80*, 1339.

(28) Pumera, M.; Scipioni, R.; Iwai, H.; Ohno, T.; Miyahara, Y.; Boero, M. *Chem.—Eur. J.* **2009**, *15*, 10851.
(29) Roy-Mayhew, J. D.; Bozym, D. J.; Punckt, C.; Aksay, I. A. *ACS Nano* **2010**, *4*, 6203.
(30) Punckt, C.; Pope, M. A.; Liu, J.; Lin, Y.; Aksay, I. A. *Electroanalysis* **2010**, *22*, 2834.
(31) Acik, M.; Lee, G.; Mattevi, C.; Pirkle, A.; Wallace, R. M.; Chhowalla, M.; Cho, K.; Chabal, Y. *J. Phys. Chem. C* **2011**, *115*, 19761.
(32) Campos-Delgado, J.; Kim, Y.; Hayashi, T.; Morelos-Gómez, A.; Hofmann, M.; Muramatsu, H.; Endo, M.; Terrones, H.; Shull, R.; Dresselhaus, M. *Chem. Phys. Lett.* **2009**, *469*, 177.
(33) Wang, Y.-L.; Zhao, G.-C. *Int. J. Electrochem.* **2011**.
(34) Ng, S. R.; Guo, C. X.; Li, C. M. *Electroanalysis* **2011**, *23*, 442.
(35) Chen, H.; Zhao, G. *J. Solid State Electrochem.* **2012**, *16*, 3289.
(36) Wen, W.; Chen, W.; Ren, Q.-Q.; Hu, X.-Y.; Xiong, H.-Y.; Zhang, X.-H.; Wang, S.-F.; Zhao, Y.-D. *Sens. Actuators, B* **2012**, *166*, 444.
(37) Punckt, C.; Pope, M. A.; Aksay, I. A. *J. Phys. Chem. C* **2013**, *117*, 16076.
(38) Zuo, X. B.; Xu, C. S.; Xin, H. W. *Electrochim. Acta* **1997**, *42*, 2555.
(39) Menshykau, D.; Compton, R. G. *Electroanalysis* **2008**, *20*, 2387.
(40) Menshykau, D.; Streeter, I.; Compton, R. G. *J. Phys. Chem. C* **2008**, *112*, 14428.
(41) Streeter, I.; Wildgoose, G. G.; Shao, L. D.; Compton, R. G. *Sens. Actuators, B* **2008**, *133*, 462.
(42) Pope, M. A.; Punckt, C.; Aksay, I. A. *J. Phys. Chem. C* **2011**, *115*, 20326.
(43) Marcano, D. C.; Kosynkin, D. V.; Berlin, J. M.; Sinitskii, A.; Sun, Z.; Slesarev, A.; Alemany, L. B.; Lu, W.; Tour, J. M. *ACS Nano* **2010**, *4*, 4806.
(44) Ferrari, A.; Robertson, J. *Phys. Rev. B* **2000**, *61*, 14095.
(45) Li, C. M.; Zang, J.; Zhan, D.; Chen, W.; Sun, C. Q.; Teo, A. L.; Chua, Y.; Lee, V.; Moochhala, S. *Electroanalysis* **2006**, *18*, 713.
(46) Gomez-Navarro, C.; Meyer, J. C.; Sundaram, R. S.; Chuvilin, A.; Kurasch, S.; Burghard, M.; Kern, K.; Kaiser, U. *Nano Lett.* **2010**, *10*, 1144.
(47) Pacile, D.; Meyer, J. C.; Rodriguez, A. F.; Papagno, M.; Gomez-Navarro, C.; Sundaram, R. S.; Burghard, M.; Kern, K.; Carbone, C.; Kaiser, U. *Carbon* **2011**, *49*, 966.
(48) Punckt, C.; Muckel, F.; Wolff, S.; Aksay, I. A.; Chavarin, C. A.; Bacher, G.; Mertin, W. *Appl. Phys. Lett.* **2013**, *102*, 023114.
(49) Liu, L.-M.; Car, R.; Selloni, A.; Dabbs, D. M.; Aksay, I. A.; Yetter, R. A. *J. Am. Chem. Soc.* **2012**, *134*, 19011.
(50) Chng, E. L. K.; Pumera, M. *Chem.—Eur. J.* **2012**, *18*, 1401.
(51) Ambrosi, A.; Pumera, M. *Chem.—Eur. J.* **2013**, *19*, 4748.
(52) Daniel, V.; Albright, J. G. *J. Chem. Eng. Data* **1995**, *40*, 519.